

Probing the Galaxy’s bars via the Hercules stream

Esko Gardner^{1*} and Chris Flynn¹

¹*Tuorla Observatory, Department of Physics and Astronomy, University of Turku, Väisäläntie 20, FI-21500, Piikkiö, Finland*

April 2010 - corrected version

ABSTRACT

It has been suggested that a resonance between a rotating bar and stars in the solar neighbourhood can produce the so called ‘Hercules stream’. Recently, a second bar may have been identified in the Galactic centre, the so called ‘long bar’, which is longer and much flatter than the traditional Galactic bar, and has a similar mass. We looked at the dynamical effects of both bars, separately and together, on orbits of stars integrated backwards from local position and velocities, and a model of the Galactic potential which includes the bars directly. Both bars can produce Hercules like features, and allow us to measure the rotation rate of the bar(s). We measure a pattern speed, for both bars, of 1.87 ± 0.02 times the local circular frequency. This is on par with previous measurements for the Galactic bar, although we do adopt a slightly different Solar motion. Finally, we identify a new kinematic feature in local velocity space, caused by the long bar, which is tempting to identify with the high velocity ‘Arcturus’ stream.

Key words: Galaxy: centre – Galaxy: kinematics and dynamics – solar neighbourhood – Galaxy: structure.

1 INTRODUCTION

The inner regions of the Milky Way contain a non-axisymmetric structure sometimes referred to as the triaxial (or boxy) bulge and/or the Galactic bar. Primary evidence for this structure are the COBE/Diffuse Infrared Background Experiment (DIRBE) near infrared (NIR) luminosity maps of the inner Galaxy (Binney et al. 1997; Bissantz & Gerhard 2002), but it has also been mapped via star counts using Two Micron All Sky Survey (2MASS) (López-Corredoira et al. 2005), 2MASS and Optical Gravitational Lensing Experiment II (OGLE-II) (Vanhollebeke et al. 2009). Typical parameters for the triaxial bulge/bar are axis ratios of 1.0:0.4:0.3, that it lies at an angle of between 10° and 40° to the line of sight to the Galactic centre (see e.g. table 1 of Vanhollebeke et al. 2009) and that its mass is of order $1 \times 10^{10} M_\odot$, (Zhao 1996; Weiner & Sellwood 1999).

It has recently been proposed (Benjamin et al. 2005) that the inner Galaxy also contains a ‘long bar’, discovered as an over-density in star count data at $4.5 \mu\text{m}$ taken in the Galactic Legacy Infrared Mid-Plane Survey Extraordinaire (GLIMPSE) survey of the Galactic centre made with *Spitzer*. Benjamin et al. (2005) measure the half-length of this bar as 4.4 ± 0.5 kpc, and lying at a position angle of $44 \pm 10^\circ$ to the line of sight to the Galactic centre. Only

the closer end of the bar was detected, as the far end would lie at apparent magnitudes fainter than the completeness limit of the survey. The long bar has been confirmed by López-Corredoira et al. (2007), who detect it via red clump stars identified from the 2MASS survey. They find a half-length of 3.9 kpc and a position angle of $43 \pm 7^\circ$, very similar to Benjamin et al. (2005). The long bar is much longer than any previously proposed bar/bulge in the Galactic centre, for which the long axis is thought to lie in the range 2.4 (e.g. Dwek et al. 1995) to 3.5 kpc (e.g. Bissantz & Gerhard 2002). Most interestingly, the long bar seems to lie at a different angle to the traditional bar/bulge (hereafter ‘Galactic bar’), for which estimates typically lie in the range 25 ± 10 degrees (Vanhollebeke et al. 2009).

Most recently, Cabrera-Lavers et al. (2007) have used wider field 2MASS data to isolate red clump stars over a wide range of Galactic longitude, showing that the long bar, the triaxial bulge and the disc can all be seen as separate structures (at least on our side of the Galaxy) with the important result that the long bar is much flatter than the bulge. The long bar is found to have a vertical scale-height of around 100 pc whereas the bulge has a vertical scale-height of 500 pc. Furthermore, the red clump stars used to trace the long bar can be used to estimate its total mass (assuming that the mass to light ratio of red clump stars is the same in the long bar as it is in the bulge) as $6 \times 10^9 M_\odot$, of the same order of the mass of the Galactic bar $1 \times 10^{10} M_\odot$, (Zhao 1996; Weiner & Sellwood 1999).

* E-mail:esgard@utu.fi

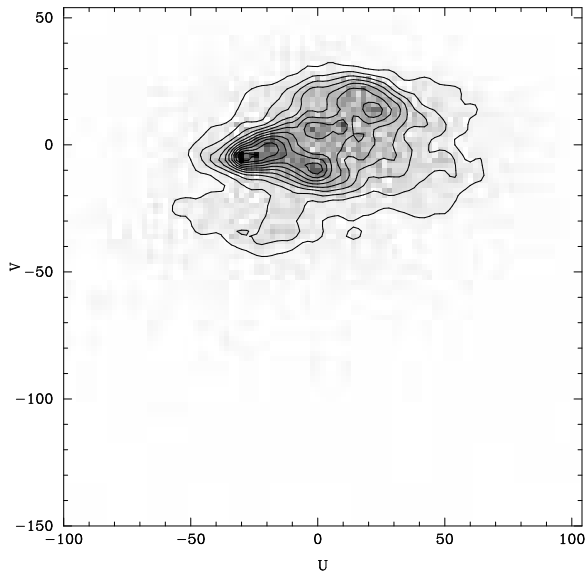


Figure 1. Local velocity space, data includes all the stars with U and V velocities from the Geneva-Copenhagen survey (Holmberg et al. 2007) and Schuster et al. (2006). The Hercules stream is the prominent feature area around $(-25, -30)$ km s $^{-1}$. The velocities have been corrected to the solar velocity from Schönrich et al. (2010)

Dehnen (2000) has shown that a bar in the inner galaxy has interesting dynamical consequences for the orbits of stars even in the solar neighbourhood, 8 kpc from the centre, due to a resonance of stellar orbits with the Outer Lindblad Resonance (OLR) of the bar. The manifestation of this resonance in our local space is the ζ Herculis stream (Eggen 1971b), or the ‘Hercules stream’ as it is usually called.

In this paper, we use a similar method to Dehnen (2000), to reexamine the dynamical effects on local disc stars of these non-axisymmetric features in the Galactic centre. We have examined both the long bar (see López-Corredoira et al. 2007) and the Galactic bar (see Bissantz & Gerhard 2002), separately, and as a dual-bar system. We adopt $R_{\odot} = 8$ kpc throughout the paper. This facilitates comparison with Dehnen (2000), who adopted the same value.

We have made a probability-statistical study of the effects of the bar(s) on local velocity space, by the means of potential theory. We will present the statistical evidence produced by various variations of the long bar-system, and a the Galactic bar-system, as well as, some interesting combined models.

2 THE HERCULES STREAM

In Fig. 1 we show local velocity space in (U, V) , where U is the velocity towards the Galactic centre and V is the velocity in the direction of Galactic rotation. The figure has been prepared using 12939 stars from the Geneva Copenhagen Survey (Holmberg et al. 2007) of abundances, ages and kinematics of nearby stars, and has been supplemented by 1535 stars from the the high velocity catalogue of Schuster et al. (2006). The bin size is 2 km s $^{-1}$, and the contours are

in 5 percent steps relative to the maximum density. The velocities have been corrected for the solar motion taken from Schönrich et al. (2010) of $(U_{\odot}, V_{\odot}) = (11.1, 12.2)$ km s $^{-1}$. The Hercules stream is the feature at approximately $(U, V) = (-25, -30)$ km s $^{-1}$. This is the feature which Dehnen (2000) identifies as having a dynamical origin as a resonance with the bar. Our simulations in this paper of a Galactic bar, long bar (and both) are primarily constrained by this feature.

The bulk of the stars in Fig. 1 belong to the complicated feature above the Hercules stream. The classically identified features in this region are the Pleiades, Sirius and Hyades streams, which occur at around $(0, -10)$, $(20, 20)$, and $(-25, -5)$ km s $^{-1}$ respectively. Further streams than those mentioned have been identified by a number of groups, but these mainly concern higher velocity stars and cannot be pointed to easily in Fig 1. One of the very interesting features at higher velocities is the Arcturus stream at $V \approx 100$ km s $^{-1}$ (for a wide range of U velocities) identified by Eggen (1971a) and discussed recently by Williams et al. (2009), who have identified it in the RAdial Velocity Experiment (RAVE) survey. The Arcturus stream may have a dynamical origin, as we show using the simulations in this paper.

3 MODELLING THE DISC AND BAR

We model the effects of a bar on local disc stars by setting up a potential describing the disc, bulge, dark halo and bar, and integrating a library of orbits passing through the Solar neighbourhood, similarly to Dehnen (2000).

We begin with the axisymmetric Galactic potential of Flynn et al. (1996). This model contains a disc, bulge and dark halo. The scale-length of disc matter (h_R) in the model is 4.4 kpc, which these days appears rather long, as recent studies of the disc scale-length give results closer to 3 kpc. Analysis of NIR data in J and K with DEep Near Infrared Survey of the Southern Sky (DENIS) give $h_R = 2.3 \pm 0.1$ kpc (Ruphy et al. 1996), while K giants seen in 2MASS give $h_R = 3.3 \pm 0.1$ kpc (López-Corredoira et al. 2002). These surveys tend to probe the scale-length of luminosity in the disc, rather than the mass, which is traced rather better via main sequence dwarfs. *Hubble Space Telescope (HST)* star counts of M dwarfs yield a disc scale-length of $h_R = 3.0 \pm 0.4$ (Gould et al. 1997). F and K dwarfs, traced in huge numbers in the 6500 deg 2 SDSS survey, yield a disc scale-length of $h_R = 2.6 \pm 0.5$ (Jurić et al. 2008). For a more complete review of the disc scale-length, see Gardner et al. (2009). We chose a disc scale-length of 3 kpc to reflect the combined observational constraints. This was straightforward and only involved modifying the Miyamoto discs from which the exponential-like disc is built up.

The surface density (Σ_{\odot}) of the new disc at the Sun’s position is $50 M_{\odot} \text{ pc}^{-2}$ and the local density ρ_{\odot} is $0.10 M_{\odot} \text{ pc}^{-3}$, consistent with observational constraints (Holmberg & Flynn 2000). The surface density of the disc as a function of Galactocentric radius is shown in Fig. 2. The new disc model has a 3 kpc scale-length, with a truncation at about 18 kpc.

The full parameters of the new disc model are shown in Table 1, along with the other parameters of the model (which are unchanged but are reproduced for clarity).

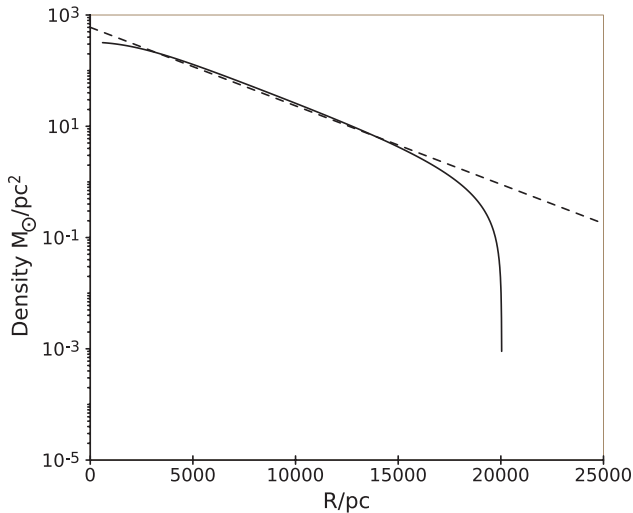


Figure 2. The surface density of the disc component (solid line) as a function of Galactocentric radius. The dashed line corresponds to an exponential density falloff, 3 kpc, which is a good fit to the model over a wide range of radii. Note that the density truncates strongly at 18 kpc.

Table 1. Parameters of the model.

Parameter	Value	Unit
V_h	220	km s ⁻¹
r_0	8.5	kpc
M_{C_1}	3	10 ⁹ M _⊙
r_{C_1}	2.7	kpc
M_{C_2}	16	10 ⁹ M _⊙
r_{C_2}	0.42	kpc
M_{d_1}	77.04	10 ⁹ M _⊙
a_{d_1}	5.81	kpc
M_{d_2}	-68.48	10 ⁹ M _⊙
a_{d_2}	17.43	kpc
M_{d_3}	26.75	10 ⁹ M _⊙
a_{d_3}	34.84	kpc
b	0.3	kpc

The equations for the axisymmetric potential are:

$$\Phi = \Phi_H + \Phi_C + \Phi_D + \Phi_{bar} \quad (1)$$

$$\Phi_H = \frac{1}{2} V_h^2 \ln(r^2 + r_0^2) \quad (2)$$

$$\Phi_C = -\frac{GM_{C_1}}{\sqrt{r^2 + r_{C_1}^2}} - \frac{GM_{C_2}}{\sqrt{r^2 + r_{C_2}^2}} \quad (3)$$

$$\Phi_{D_n} = \frac{-GM_{D_n}}{\sqrt{(R^2 + (a_{d_n} + \sqrt{(z^2 + b^2)})^2)}}, \quad (4)$$

where $\Phi_D = \sum_{n=1}^3 \Phi_{D_n}$, $r = x^2 + y^2 + z^2$, and $R = x^2 + y^2$.

We have used a different method to modelling the bar as was adopted in Dehnen (2000) and Minchev et al. (2007). Instead of modelling the bar as a local quadrupole perturbation to the potential, we model the bar directly in the inner galaxy. This means that orbits of stars entering into the in-

Table 2. Default simulation parameters.

Parameter	Value	Unit
Galactic Bar		
Angle	25	°
Dimensions	3.5:1.4:1.0	kpc
Mass	10	10 ⁹ M _⊙
Pattern Speed	55.9	km s ⁻¹ kpc ⁻¹
Local standard of rest	239	km s ⁻¹
OLR	1.87	
Long Bar		
Angle	43	°
Dimensions	3.9:0.6:0.1	kpc
Mass	6	10 ⁹ M _⊙
Pattern Speed	54.9	km s ⁻¹ kpc ⁻¹
Local standard of rest	235	km s ⁻¹
OLR	1.87	

ner disc regions and even passing through the bar are much more accurately modelled, even if it is computationally far more expensive.

The bar is modelled as a Ferrers $n = 2$ potential, as laid out by Pfenniger (1984), and as such, is a triaxial ellipsoid. The equations for the bar are too complex to present here (for full details see Pfenniger 1984). The bar rotates as a rigid body.

A bar is specified by its three axis lengths, its mass, its angular (or pattern) speed and its angle to the line connecting the Galactic centre and the Sun.

We have two standard bars, with parameters taken from López-Corredoira et al. (2007) and from Bissantz & Gerhard (2002). The dimensions of the ‘long bar’ are (3.9:0.6:0.1) kpc, with a mass of 6 10⁹ M_⊙ and an angle of 43°. The ‘Galactic bar’ has dimensions of (3.5:1.4:1.0) kpc, a mass of 10¹⁰ M_⊙ and an angle of 25°. These masses correspond to a Dehnen (2000) α value of 0.0037, for the long bar case, and 0.0040, for the Galactic bar case. Note that in the simulations we do not vary the dimensions of the respective bars, only the mass and position angle.

An important parameter is the pattern speed of the bar. Following Dehnen (2000) and Minchev et al. (2007), we parametrise the bar’s pattern speed by the OLR, i.e. by the ratio of the period of a star with velocity of the local standard of rest (LSR) in a given Galactic model to the period of rotation of the bar.

The definition of the LSR is straightforward in axisymmetric models of the Galaxy, but needs to be redefined slightly once we have added a bar to the model. In the presence of a bar, a star can no longer follow a circular orbit at the solar radius, but rather oscillates around a mean radius. For typical bar parameters, the oscillation is up to 10 km s⁻¹, compared to a mean velocity of 220 km s⁻¹ in typical models. For each model run in our simulations, we determine, experimentally, at what velocity a star, which starts at the Solar position, would have a mean orbital radius of 8 kpc. Integration is carried out for 10 Gyr, so that the effect of the effect of the angle of the bar is averaged out. This is defined as the LSR for that model.

4 SIMULATIONS AND METHODS

The basic simulation approach is to model the appearance of local velocity space using the method described by Dehnen (2000), a ‘backward restricted N -body method’. The idea is to trace a library of orbits starting from the solar neighbourhood backwards over some fixed time (typically 1 Gyr), and use the known density distribution and velocity distribution of the disc to reconstruct the velocity distribution of stars in the solar neighbourhood.

We introduce two refinements, firstly, a more realistic representation of the bar potential and secondly, we use observational constraints on the velocity dispersion and asymmetric drift of stars in the Galactic disc over a wide range of Galactocentric radius obtained by Lewis & Freeman (1989). In practise, this latter refinement is not very different to the approach adopted by Dehnen (2000), (simple exponential functions of stellar density and radial velocity dispersion for the old stellar disc) and indeed we find that we reproduce his results quite well when we adopt a bar similar to his. Our simulations are in two dimensions (2D), as in Dehnen (2000).

The initial conditions are set by a velocity-grid, of 100 by 100 elements in the UV -velocity plane, covering $U = -100$ to 100 km s^{-1} , and $V = -150 \text{ km s}^{-1}$ to $V = 50 \text{ km s}^{-1}$, in steps of 2 km s^{-1} . A tracer with the UV -velocity selected from the grid is then set into motion, following the tracer backwards in time over a period of 1 Gyr, tracking its position every 1 Myr. The initial position is selected as the solar position (8 kpc), and both the z -coordinate and the W -velocity are set to zero. The initial velocity in the rotational direction V is, of course, relative to the LSR for particular model being tested.

Statistically, we use a density and velocity-based system, where a weight value corresponds to a 8 kpc-centric exponential distribution, and a Gaussian velocity-distribution, with standard deviations as described in Lewis & Freeman (1989). The V -velocity is corrected back to a ‘true’ V -velocity using the LSR of the position and the asymmetric drift (Lewis & Freeman 1989).

5 RESULTS

We examine in this section the effects of both the ‘Galactic bar’ and the ‘long bar’ on local velocity space. We vary the bar mass, value of the OLR (i.e. the pattern speed of the bar), and the angle of the bar. Finally, we look at the effects of including both bars at the same time.

5.1 Effect of the mass of the Galactic bar

We begin by running the standard model of the ‘Galactic bar’ but varying its mass over a range of 1 to $10 \times 10^9 M_{\odot}$, showing the results in Fig. 3. The OLR for this case is 1.87. The variations of mass within one order of magnitude have prominent effects. As found by Dehnen (2000) we find that a Hercules-like feature arises in local velocity space in the presence of a bar. We will henceforth refer to this as a secondary feature in velocity space, with the primary feature (above it) containing most of the stars. The effect of

increasing the mass of the bar is similar to that found by Dehnen (2000), with the strength of the secondary feature increasing (and the depth of the resonance gap between the secondary feature and primary feature also growing). The secondary component becomes more ellipsoidal, as mass is increased, and, as expected, becomes more prominent. Also, the position of the secondary feature moves to more negative V velocities as the mass is increased. While it is clear that something like the Hercules feature can be generated by this bar, the detailed match is not yet perfect. In Fig. 1, the Hercules feature is found at $(U, V) = (-25, -30) \text{ km s}^{-1}$. In the simulations, the generated feature approaches this location for the higher mass models, but at the expense of generating a sharp ‘tail’ of stars at positive U values spreading outward from the primary feature. This tail of stars is also seen in the Dehnen (2000) and Minchev et al. (2007) simulations, and increases with the mass of the adopted bar. Such a tail, if present at all in the observational data (Fig. 1) is quite weak. Apart from this tail, the generated feature is fairly consistent with various estimates of bar mass where they are consistently around and over $10^{10} M_{\odot}$ (see e.g. Zhao 1996; Weiner & Sellwood 1999).

5.2 Long bar

We next look at the ‘long bar’ case. We adopt the standard model for its dimensions and initial position angle and vary only the mass. These models all give a Hercules-like secondary feature, similar to the Galactic bar case. The effect of varying its mass on local velocity space is shown in Fig. 4. One can see that mass takes a significant role in the division of the primary and secondary feature, where the secondary is stronger with increasing mass. Again, these plots superficially resemble the real local velocity space (Fig. 1) but not in detail. The position of the secondary feature tends to be at too high V velocities and the tail of stars at high U values also appears for the higher mass models.

One very interesting ‘tertiary’ feature appears with the long bar, located at $V = -80$ to -100 km s^{-1} . The tertiary feature becomes more prominent as mass increases. This feature is not seen in the Galactic bar simulations (Fig. 3). We will return to this feature in section 5.4.

5.3 Pattern speed of the bar

As shown by Dehnen (2000) and Minchev et al. (2007), the position of the Hercules feature is quite dependent on the adopted pattern speed of the bar, parametrised by the OLR. The feature can therefore be used to measure the pattern speed of the bar. Dehnen (2000) finds that the feature can be fit by an OLR of 1.85 ± 0.15 , using similar simulations to ours. Minchev et al. (2007) find a similar and more tightly constrained value of the OLR of 1.87 ± 0.04 , using similar simulations as here but also from constraints implied by the locally measured Oort constant C .

Our standard model for both the Galactic and long bars assumes an OLR of 1.87. For the Galactic bar case, the effect of shifting from an OLR value of 1.87 to 1.90 is shown in Fig 5. The secondary feature shifts by about 5 km s^{-1} to more negative V velocities. A more detailed view of this is shown for the long bar case in Fig. 6, where we have varied the

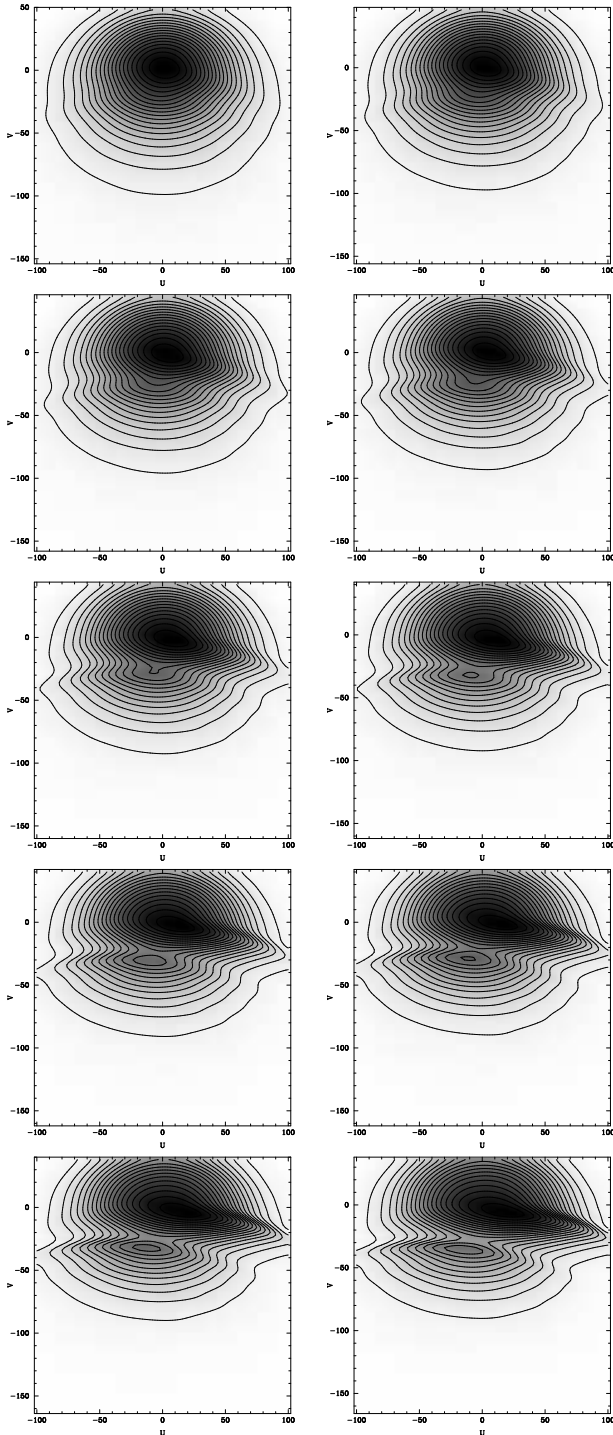


Figure 3. Effect on local velocity space of varying the mass of the Galactic bar, from 10^9 to $10^{10} M_{\odot}$ in increments of $10^9 M_{\odot}$. For other simulation parameters see Table 2.

value of the OLR ranging from 1.83 to 1.95. The secondary feature shifts quite markedly away from the primary feature over this range of assumed OLR values. We derive a best fitting OLR of 1.87 ± 0.02 , assuming that the position of the secondary feature is at $V = -30 \pm 5 \text{ km s}^{-1}$.

Our determination of the OLR value for the bar is in agreement with Dehnen (2000) and Minchev et al. (2007) within the error bars. We note that our value about the

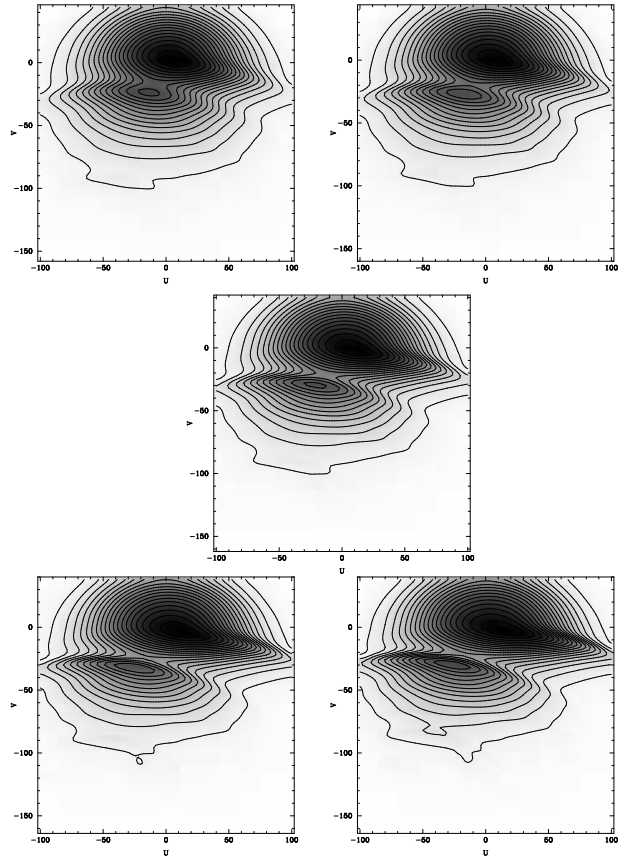


Figure 4. Variations of velocity space with different values of long bar mass. Masses are 4, 5, 6 (middle), 7, and $8 \times 10^9 M_{\odot}$. For other simulation parameters see Table 2.

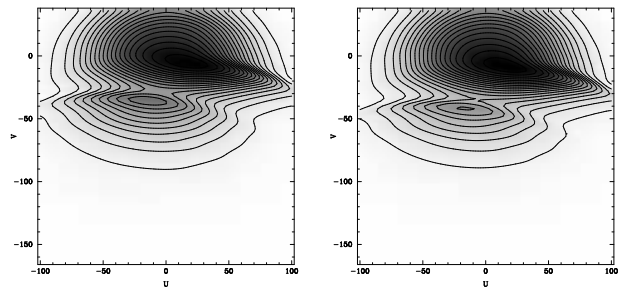


Figure 5. Variation of velocity space with a Galactic bar model, OLR values of 1.87 and 1.90.

same as theirs, even though we adopt the solar motion of Schönrich et al. (2010), which shifts this feature by 7 km s^{-1} to more positive V velocities in the observational plane (the Hercules feature is centred on about $V = -35 \text{ km s}^{-1}$ with the solar motion adopted by Dehnen (2000), rather than at $V = -30 \text{ km s}^{-1}$ as in our Fig. 1. Had we adopted the older solar motion, we would obtain an OLR of 1.90 ± 0.03 .

5.4 Bar angle

Dehnen (2000) used the Hercules stream to probe the angle of the bar, deriving an angle of 25° . This is to be compared to the observational evidence for the (Galactic bar) angle, which lies in the range 20° to 40° . We probe the effect of bar

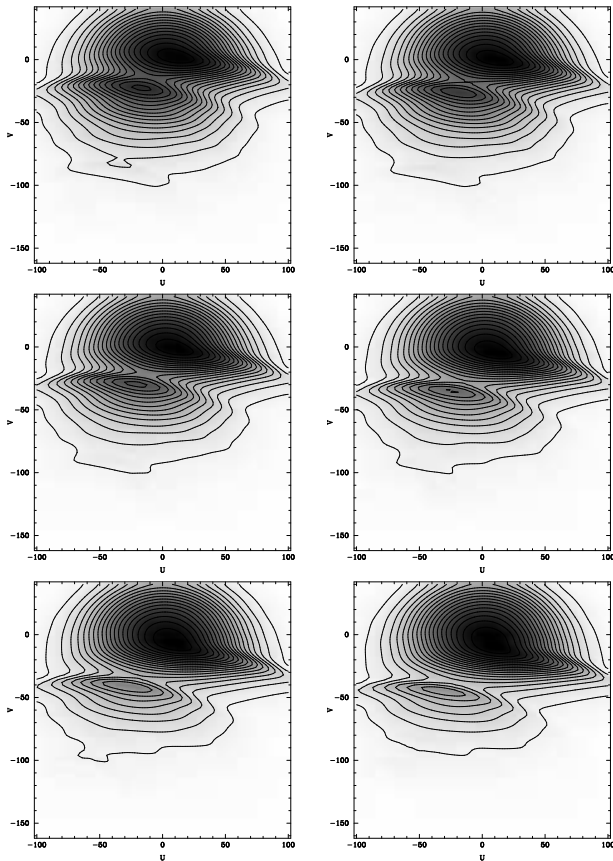


Figure 6. Effect on local velocity space with different values of for the OLR for the long bar case. Values are 1.83, 1.85, 1.87, 1.90, 1.93, and 1.95, from left to right, top to bottom. There is a clear shift in the position of the secondary feature to lower V velocity as the OLR increases, allowing a determination to be made of the pattern speed of the bar.

angle as well, for both the Galactic bar and long bar cases. As found by Dehnen (2000), the effect is to change of the position of the secondary feature to towards more negative values of U and more positive values of V with increasing bar angle, and also to change the strength of the feature, as seen in Figs 7 and Fig. 8. However, these changes are rather subtle and we consider them too weak to constrain the bar angle.

The tertiary feature is clearly dependant on bar angle, both for the long bar case and the Galactic bar case. The feature appears in both cases when the initial bar angle is greater than 40° . The orbits of stars in this feature are highly eccentric and take them to within 2 kpc of the Galactic centre, ideal for direct interaction with a bar. This accounts for why bar angle is important to the generation of the tertiary feature.

There is a stream in the Solar neighbourhood at about this velocity, $V \sim -100 \text{ km s}^{-1}$, the Arcturus stream (Eggen 1971a). The stream has recently been recovered in the RAVE survey by Williams et al. (2009). Williams et al. (2009) argue against an accretion origin for this stream, because its stars have a wide range of metallicity, so that the accreted system would have to have an unreasonably high mass, perhaps as large as the Large Magellanic Cloud (LMC). It is interesting that our simulations show that a dynamical ori-

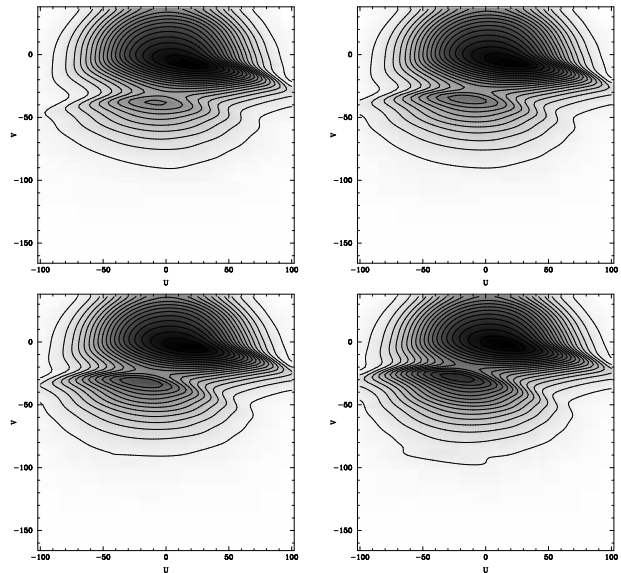


Figure 7. Variation of Galactic bar angle, 15° , 25° , 35° , and 45°

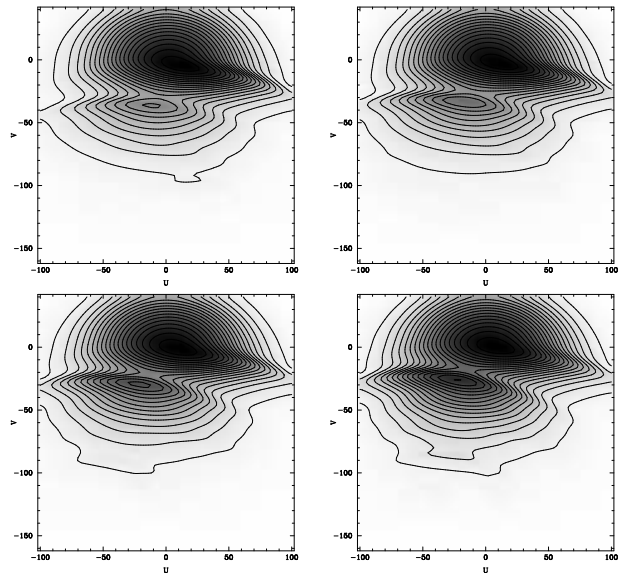


Figure 8. Variation of long bar angle, 23° , 33° , 43° , and 53° .

gin for the stream is plausible. Streams with a dynamical origin are expected to have a wide range of metallicity, as wide as the stars of its parent population. If so, the more plausible bar for originating this stream is the long bar, because its measured bar angle is 43° . The Galactic bar could also produce this stream, but it would have to also be at an angle of about 45° , whereas most studies find that it lies much closer to the line of sight to the Galactic centre, at about 20° (Vanhollebeke et al. 2009).

5.5 Integration time

We have chosen an integration time of 1 Gyr, but this choice is somewhat arbitrary. Fig. 9 shows the effects of adopting shorter and longer integration times of 500 Myr and 2 Gyr for the long bar.

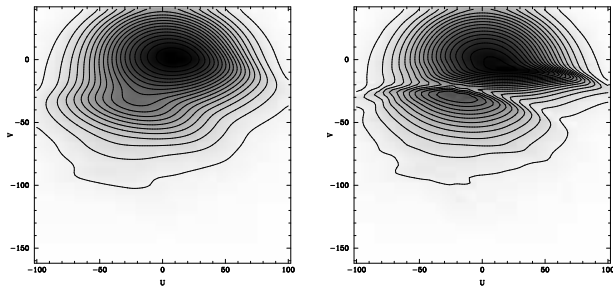


Figure 9. Variation in integration time, 500 Myr, and 2 Gyr, using the long bar.

After 500 Myr, the secondary feature has started forming but is not yet prominent. This represents about 4 bar rotations, and it is not surprising that it takes some time for the resonance with the bar to develop the trough between the primary and secondary features. After 2 Gyr we can see the stronger splitting of the primary and secondary feature, with the resonance-area clearing, as well as the primary feature tailing out to more positive U . Simulations as long as this assume of course that the bar has existed for 2 Gyr with the same parameters, in particular that the rotation rate and mass have not changed during this time. Our choice of 1 Gyr is meant to allow structure enough time to develop, while not taxing the credibility of bar properties being very long lived in galaxies like the Milky Way. Fux (2001) has pointed out a potential difficulty with the backwards integration technique used here. He finds that as one integrates further backwards in time, increasingly spurious structures develop in the UV -plane. We find no such behaviour over approximately 16 periods of the bar (Fig. 9). We are confident in our 1 Gyr timescale, for interpreting the simulations.

5.6 Dual bar models

Our simulations have shown that both the Galactic bar, and the newly discovered ‘long bar’ can generate features in velocity space which are superficially similar to those seen in the Solar neighbourhood, in particular the Hercules stream. We now investigate the effect of including both bars.

We show a selection of dual bar models in Fig. 10. We begin with both bars having the same OLR - i.e. the two bars have the same pattern speed and rotate together. The upper panels of Fig. 10 show the local effect on phase space for OLR values of 1.87 and 1.90. The overwhelming impression here is that the main feature in phase space is driven to large values of U , inconsistent with observations. The main cause for this is simply the large amount of mass which now resides in the Galactic centre, in these cases $1.6 \cdot 10^{10} M_{\odot}$. Similar behaviour is seen even for cases with a single bar, when the mass of the bar exceeds about $10^{10} M_{\odot}$. More than this much mass and the bar(s) starts to generate an unacceptable amount of activity on the Solar neighbourhood (U, V) distribution, typically pushing stars to too large values of U .

Two decoupled scenarios were tested, with one of the bars at an OLR of 1.50 and the other at 1.87. These are shown in the middle panels of Fig. 10. On the right, the Galactic bar has an OLR of 1.50, while the long bar has an OLR of 1.50 on the left. Again, the total mass in the

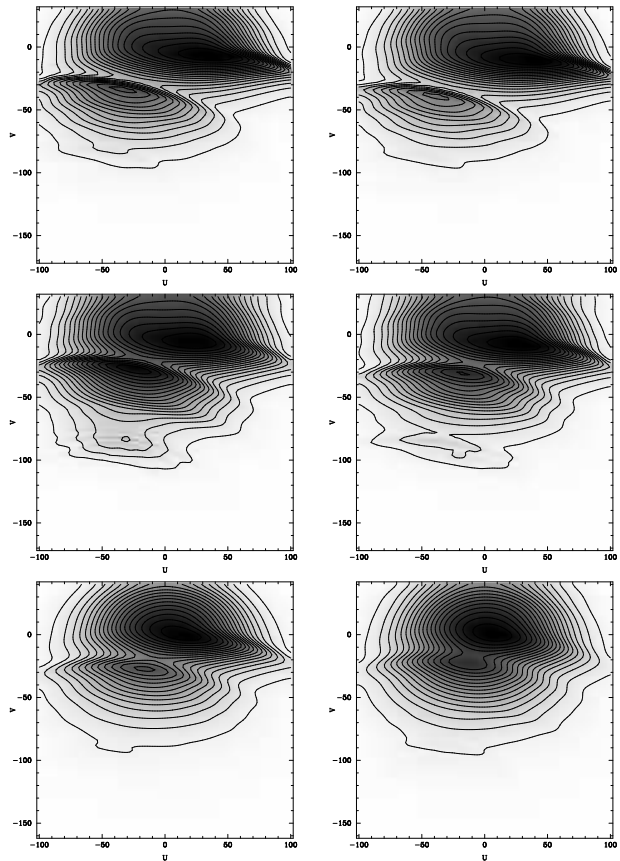


Figure 10. Dual bar models, phase-locked 1.87 and 1.90 (top), unlocked, long at 1.87, galactic at 1.5 (middle left), long at 1.5 galactic at 1.87 (middle right), half-mass locked at 1.87 (bottom left), half-mass unlocked long at 1.87, galactic at 1.5 (bottom right).

two bars is generating significant structure in local velocity space, with the same problem of too many stars being shifted into a tail of high U velocities. In addition, the tertiary feature at $V \sim -80$ becomes very prominent, as the chances of an interaction with either bar is now higher. We tested this by running single-bar models with an OLR of 1.5, which results in no secondary or tertiary feature for the Galactic bar case, and in the long bar case it causes no secondary and a very weak tertiary, such as seen in other single-bar simulations of the long bar. Both the upper and middle panels show more structure than really exists in the Solar neighbourhood, primarily because too much mass is assigned to the bar structures in the inner Galaxy. To alleviate this problem, we tested a scenario where the masses of both bars are simply halved. This is shown in the lower panels of Fig. 10. On the left, the bars both have an OLR of 1.87, while on the right, the bars are unlocked, with the Galactic bar at an OLR of 1.5 and the long bar with an OLR of 1.87. Reducing the mass brings the simulations into much better agreement with the observations, although the secondary feature is at a too high V velocity. This can be remedied by shifting to a higher value of 1.90 for the OLR.

6 DISCUSSION & CONCLUSIONS

We have performed simulations of the effects of bars in the inner Galaxy on the distribution of stars in velocity space near the Sun. Our simulations are similar to those of Dehnen (2000) and Minchev et al. (2007), in which a large library of orbits of stars passing through the Solar neighbourhood are performed in a model of the Galactic potential including a bar. These earlier studies showed that the Hercules stellar stream in the solar neighbourhood could be the result of a resonance of stellar orbits with a fast moving bar (i.e. with a co-rotation with the Galactic disc not much beyond the end of the bar). Both Dehnen (2000) and Minchev et al. (2007) find that the Hercules stream can be used to constrain the rotation rate and angle of the bar.

Our motivation to reexamine this is the recent discovery that the Galaxy may contain a second bar, in addition to the traditional Galactic bar, by Benjamin et al. (2005) and López-Corredoira et al. (2007). These authors have found a ‘long bar’ in the Galactic centre. It is quite different to the Galactic bar, being highly flattened (semi-major axes of 3.9, 0.6 and 0.1 kpc as compared to 3.5, 1.4 and 1.0 kpc). Furthermore, it is aligned at an angle of about 43 degrees to the line of sight to the Galactic centre, as opposed to about 20 degrees for the Galactic bar. For the Galactic bar we adopt a mass of $10^{10} M_{\odot}$ (Zhao 1996; Weiner & Sellwood 1999) and for the long bar $6 \times 10^9 M_{\odot}$ (López-Corredoira et al. 2007). The long bar has a mass quite comparable to the traditional bar.

We have simulated the effects of the long bar, as well as the Galactic bar, and both bars, on the velocities of stars in the Solar neighbourhood. Rather than simulating bars as a quadrupole perturbation in the local Galactic potential, we simulate the bars with a Ferrers potential (which generates a triaxial ellipsoidal density distribution). This is computationally more expensive, but allows for more accurate modelling of a bar as a whole, especially for stars passing through, or trapped in, a bar. The simulations are performed in 2-D, although the model itself allows 3-D simulations.

We confirm the basic picture that the Hercules stream can be generated by a resonance between local stars and the bar. Both the long bar and the Galactic bar produce Hercules-like features in the Solar neighbourhood. The position of the Hercules stream in the simulations is found to depend on the mass of the bar, the rotation rate of the bar, and rather weakly, on the angle of the bar. The geometry of the bars is not very important either, since both bars generate Hercules-like streams.

We measure the rotation rate of the bars from the position of the Hercules stream, finding that both bars can produce acceptable fits to of the (U, V) velocities of nearby stars. We measure the rotation rate of both bars via the Outer Lindblad Resonance value they produce (i.e. by the ratio of the period of a star with velocity of the Local Standard of Rest in a given Galactic model to the period of rotation of the bar). We measure values of 1.87 ± 0.02 for the OLR of both the Galactic bar and the long bar. This value gives a pattern speed of 55.9 and $54.9 \text{ km s}^{-1} \text{ kpc}^{-1}$, respectively, for the Galactic bar and long bar. This puts the corresponding co-rotation, for the long bar, as defined by its potential model, at the approximate tip of the bar, 3.9 kpc. For the Galactic bar, our model produces no co-rotation radius. It

should be noted however that this value is sensitive to the assumed Solar motion. We assume the Solar motion recently derived by Schönrich et al. (2010). Had we adopted the Solar motion used by Dehnen (2000), we would have derived a value of 1.90 ± 0.03 . Both of these derived values are in reasonable agreement with Dehnen (2000)’s determination of 1.85 ± 0.15 and Minchev et al. (2007)’s determination of 1.87 ± 0.04 .

After looking at the effects of each bar alone, we tried putting both bars into the modelling. The effects on local velocity space are quite dramatic, as we have now added quite a lot of mass in a non-axisymmetric component to the Galactic centre. In particular, these simulations produce a striking tail of stars in the Solar neighbourhood at high U velocities, inconsistent with observations. The simple expedient of halving the mass of both bars produces much better fits to the data. On the basis of these experiments then, if there are two bars in the Galactic centre, we wonder whether the mass estimates of each bar include material from the other bar, and are perhaps overestimates. This offers a challenge to observational studies of the bar masses.

Finally, we have found that an additional feature in local velocity space can arise under some conditions, especially for the long bar case. A weak stream of stars can form at about $V \sim -100$ and $U < 0 \text{ km s}^{-1}$. We believe this is due to a direct interaction of such stars with the bar, rather than a resonance with the bar. It is tempting to associate this feature with the known Arcturus stream at $V \sim -100 \text{ km s}^{-1}$ (Williams et al. 2009) in the Solar neighbourhood. Thus, a dynamical origin for the stream is possible, whereas people have mainly discussed accretion origins (of a satellite galaxy) to date.

We point out that our method has shortcomings. Firstly, the simulations are in 2-D, and while this is almost certainly acceptable for typical disc stars with near circular orbits, full 3-D simulations may be needed for features like that which we associate with the Arcturus stream. In addition, there are no spiral arms or other non-axisymmetric components, besides the bars, in the modelling, and these may be responsible for additional complexity in local velocity space which we cannot model. We are not affected by the problems of long-term backwards integration as mentioned in Fux (2001). Compared to earlier studies, we try to more accurately represent the Galaxy’s observed properties, such as local densities and bar geometry. The model also lets us look at direct interaction, as well as resonances, this is especially important for high velocity stars (e.g. those in the Arcturus stream), where they have high enough eccentricities to enter the inner parts of the Galaxy. The model also makes it possible, in the future, to fully study the 3D impact of the bar(s).

ACKNOWLEDGEMENTS

The authors wish to thank Professor Kimmo Innanen for starting out this project, as well as Professor Daniel Pfenniger for providing his code for the bar potential. We also wish to thank Burkhard Fuchs and the referee for insightful comments. EG acknowledges the financial support of the Finnish Cultural Fund and the Finnish Graduate School in

Astronomy and Space Physics. CF acknowledges financial support by the Academy of Finland.

REFERENCES

- Benjamin R. A., Churchwell E., et al. 2005, *ApJL*, 630, L149
- Binney J., Gerhard O., Spergel D., 1997, *MNRAS*, 288, 365
- Binney J., Tremaine S., 2008, *Galactic Dynamics: Second Edition*. *Galactic Dynamics: Second Edition*, by James Binney and Scott Tremaine. ISBN 978-0-691-13026-2 (HB). Published by Princeton University Press, Princeton, NJ USA, 2008.
- Bissantz N., Gerhard O., 2002, *MNRAS*, 330, 591
- Cabrera-Lavers A., Hammersley P. L., González-Fernández C., López-Corredoira M., Garzón F., Mahoney T. J., 2007, *A&A*, 465, 825
- Carlson B. C., 1994, *ArXiv Mathematics e-prints*
- Chandrasekhar S., 1969, *Ellipsoidal figures of equilibrium*. The Silliman Foundation Lectures, New Haven: Yale University Press, 1969
- Dehnen W., 2000, *AJ*, 119, 800
- Dwek E., Arendt R. G., Hauser M. G., Kelsall T., Lisse C. M., Moseley S. H., Silverberg R. F., Sodroski T. J., Weiland J. L., 1995, *ApJ*, 445, 716
- Eggen O. J., 1971a, *PASP*, 83, 271
- Eggen O. J., 1971b, *PASP*, 83, 251
- Flynn C., Sommer-Larsen J., Christensen P. R., 1996, *MNRAS*, 281, 1027
- Fux R., 2001, *A&A*, 373, 511
- Gardner E., Innanen K. A., Flynn C., 2009, in J. Andersen, J. Bland-Hawthorn, & B. Nordström ed., *IAU Symposium Vol. 254 of IAU Symposium, Dynamical effects of the long bar in the Milky Way*. p. 21P
- Gould A., Bahcall J. N., Flynn C., 1997, *ApJ*, 482, 913
- Holmberg J., Flynn C., 2000, *MNRAS*, 313, 209
- Holmberg J., Nordström B., Andersen J., 2007, *A&A*, 475, 519
- Jurić M., Ivezić Ž., Brooks A., Lupton R. H., Schlegel D., et al. 2008, *ApJ*, 673, 864
- Lewis J. R., Freeman K. C., 1989, *AJ*, 97, 139
- López-Corredoira M., Cabrera-Lavers A., Garzón F., Hammersley P. L., 2002, *A&A*, 394, 883
- López-Corredoira M., Cabrera-Lavers A., Gerhard O. E., 2005, *A&A*, 439, 107
- López-Corredoira M., Cabrera-Lavers A., Mahoney T. J., Hammersley P. L., Garzón F., González-Fernández C., 2007, *AJ*, 133, 154
- Minchev I., Nordhaus J., Quillen A. C., 2007, *ApJL*, 664, L31
- Pfenniger D., 1984, *A&A*, 134, 373
- Ruphy S., Robin A. C., Epchtein N., Copet E., Bertin E., Fouque P., Guglielmo F., 1996, *A&A*, 313, L21
- Schönrich R., Binney J., Dehnen W., 2010, *MNRAS*, 403, 1829
- Schuster W. J., Moitinho A., Márquez A., Parrao L., Covarrubias E., 2006, *A&A*, 445, 939
- Vanhollebeke E., Groenewegen M. A. T., Girardi L., 2009, *A&A*, 498, 95
- Weiner B. J., Sellwood J. A., 1999, *ApJ*, 524, 112
- Williams M. E. K., Freeman K. C., Helmi A., the RAVE collaboration 2009, in J. Andersen, J. Bland-Hawthorn, & B. Nordström ed., *IAU Symposium Vol. 254 of IAU Symposium, The Arcturus Moving Group: Its Place in the Galaxy*. pp 139–144
- Zhao H., 1996, *MNRAS*, 278, 488